Assessing the Impact of Cumulus Convection and Turbulence Parameterizations on Typhoon Precipitation Forecast

Yueya Wang[1], Haobo Li[2], Xiaoming Shi[1] , and **Jimmy C. H. Fung[1,3]**

[1]Division of Environment and Sustainability, Hong Kong University of Science and Technology, Hong Kong, China, [2]Department of Computer Science and Engineering, Hong Kong University of Science and Technology, Hong Kong, China, [3]Department of Mathematics, Hong Kong University of Science and Technology, Hong Kong, China

Abstract Improving typhoon precipitation forecast with convection-permitting models remains challenging. This study investigates the influence of cumulus parameterizations and turbulence models, including the Reconstruction and Nonlinear Anisotropy (RNA) turbulence scheme, on precipitation prediction in multiple typhoon cases. Incorporating the cumulus and RNA schemes increases domain-averaged precipitation, improves recall scores, and lowers relative error across various precipitation thresholds, which is substantial in three out of four studied typhoon cases. Applying appropriate cumulus parameterization schemes alone also contributes to enhancing heavy precipitation forecasts. In Typhoon Hato, the RNA and Grell-3 schemes demonstrated a doubled recall rate for extreme rainfall compared to simulations without any cumulus scheme. The improved forecasting ability is attributed to the RNA's capacity to model dissipation and backscatter. The RNA scheme can dynamically reinforce typhoon circulation with upgradient momentum transport in the lower troposphere and enhance the buoyancy by favorable heat flux distribution, which is conducive to developing heavy precipitation.

Plain Language Summary Enhancing the forecast accuracy of typhoon-induced rainfall prediction with numerical weather prediction models is still challenging. This study focused on the impact of cumulus convection schemes and a new turbulence scheme named the Reconstruction and Nonlinear Anisotropy (RNA) scheme on the precipitation forecast performance when typhoons hit. We found that the convection and the RNA schemes help predict more rain on average and make our predictions more accurate, especially regarding heavy rainfall. Still, it also leads to an overestimation of the precipitation. In addition, applying the cumulus and RNA scheme is beneficial in keeping the typhoon structure and intensity at a lower sea level pressure. This improvement in generating intense convections is due to the optimized configuration of the dissipation and backscattering caused by the subgrid-scale turbulence.

1. Introduction

Tropical cyclones frequently affect South China, causing extreme precipitation and winds leading to landslides and flooding, resulting in substantial economic damage and loss. Despite progress in numerical weather prediction, accurately forecasting typhoon precipitation intensities remains challenging. Cumulus parameterization, which represents subgrid convection, is crucial in precipitation forecasting. Previous studies suggest that disabling the cumulus scheme is appropriate when the grid scale is less than 4 km, as the explicit microphysics scheme and model dynamics are expected to resolve cloud and precipitation processes (Skamarock et al., 2008; Weisman et al., 1997). However, whether cumulus parameterization should be applied at kilometer-scale resolution remains controversial in the tropical cyclone community, because this resolution falls within the gray zone, where both resolved and subgrid processes can contribute to turbulence (Boutle et al., 2014; Gerard, 2007; Shi, Chow, et al., 2019; Wyngaard, 2004). Sun et al. (2013, 2014) performed sensitivity experiments to analyze the simulated Tropical Cyclone (TC) intensity for Typhoon Shanshan using different cumulus parameterization schemes under the gray-zone resolution by varying their resolution from 4 to 10 km. They suggest that a suitable cumulus scheme can enhance tropical cyclone convergence. Conversely, Yu and Lee (2011) discovered that simulations would overpredict the area-averaged precipitation rate without employing convective parameterization. Recent studies further indicated that the scale-aware cumulus scheme can improve precipitation prediction (Gao et al., 2017; Mahoney, 2016). Shi and Wang (2022) demonstrated that simulations without cumulus schemes

Writing – review & editing:
Yueya Wang, Haobo Li

underestimate precipitation and overall performance for extreme rainfall prediction. Given the uncertain impacts of utilizing cumulus schemes in high-resolution simulations on typhoon precipitation prediction, further evaluation of the necessity and effect of cumulus convection in kilometer-scale simulations with additional typhoon cases is needed.

Previous studies pointed out that the equivalent potential temperature exhibits a significant horizontal gradient in TCs, indicating that subgrid-scale mixing should be considered in high-resolution tropical cyclone simulations (Houze Jr, 2014). Although the traditional planetary boundary layer (PBL) scheme remains valid for subgrid-scale turbulence at the kilometer-scale resolution, with the gray zone bound being ≥100 m for the PBL scheme, horizontal subgrid-scale turbulence is not accounted for in conventional PBL schemes or cumulus parameterizations, assuming the environment is horizontally homogeneous at subgrid scales.

In the Weather Research and Forecasting (WRF) model, the horizontal turbulence can be represented by a gradient-diffusion scheme, such as the two-dimensional Smagorinsky model (Zhou et al., 2017). However, the Smagorinsky scheme does not allow backscatter, which is observed according to in situ measurements and LES simulation results (Carper & Porté-Agel, 2004; Shi et al., 2018). Chow et al. (2005) developed the dynamic reconstruction model (DRM) of turbulence based on an explicit filtering framework, dividing the subfilter-scale turbulence flux into resolvable subfilter-scale (RSFS) and subgrid-scale (SGS) components. Shi and Wang (2022) replaced the SGS part with the nonlinear backscatter and anisotropy (NBA) model and applied it to represent horizontal turbulence, their results for simulating Typhoon Vicente indicated that it can enhance the precipitation with the optimal configuration of dissipation and backscattering. Nevertheless, studies examining the effects of cumulus schemes and horizontal turbulence on typhoon precipitation at the gray-zone scale are still limited. In this study, we further investigate the performance and necessity of considering vertical and horizontal turbulence mixing at kilometer-scale resolution by testing the impact of a cumulus parameterization and RNA scheme on precipitation forecasting with multiple typhoon cases.

2. Methods and Experiment Design

2.1. Turbulence Schemes

The horizontal stress in the Smagorinsky scheme is represented as

$$\tau_{ij} = -K_h D_{ij} \tag{1}$$

the K_h and D_{ij} are the horizontal eddy viscosity and deformation tensor, respectively. In the WRF model, the turbulent scalar flux has a similar expression as Equation 1, with the scalar diffusivity being divided by the turbulent Prandtl number Pr = 1/3.

In the RNA scheme, the subfilter-scale turbulence stress is (Shi, Chow, et al., 2019):

$$\tau_{ij} = \tau_{ij}^{\text{RSFS}} + \tau_{ij}^{\text{SGS}} \tag{2}$$

The RSFS is computed by adopting the explicit filtering-based RSFS model of DRM (Chow et al., 2005; Kirkil et al., 2012; Shi et al., 2018) as

$$\tau^{\text{RSFS}} = \overline{u_i^\star u_j^\star} - \overline{u_i^\star}\ \overline{u_j^\star} \tag{3}$$

Following the approximate deconvolution method (ADM) (Stolz & Adams, 1999; Stolz et al., 2001), the $u^\star$ is:

$$u^\star = \overline{u}_i + (I - G)\overline{u}_i + (I - G)[(I - G)\overline{u}_i] + \dots, \tag{4}$$

where I is the identity operator and G is the explicit filter. The reconstructed velocity retains the first term only and is estimated as the grid velocity; the overbar denotes a top-hat filter.

Table 1
Experiment Design for Each Typhoon Case With Different Schemes

Simulation	Cumulus scheme (outer domain)	Cumulus scheme (inner domains)	Horizontal turbulence scheme
GF-GF-R	Grell–Freitas	Grell–Freitas	RNA
GF-GF-S	Grell–Freitas	Grell–Freitas	Smagorinsky
GF-GF-N	Grell–Freitas	Grell–Freitas	None
GF-N-N	Grell–Freitas	None	None
GF-N-R	Grell–Freitas	None	RNA
G3-G3-R	Grell-3	Grell-3	RNA
G3-G3-S	Grell-3	Grell-3	Smagorinsky
G3-G3-N	Grell-3	Grell-3	None
G3-N-N	Grell-3	None	None
G3-N-R	Grell–3	None	RNA

The nonlinear backscatter and anisotropy (NBA) model is adopted here to consider the backscattering effect (Kosović, 1997; Mirocha et al., 2010; Shi et al., 2018). Therefore, the SGS term in the DRM model is expressed as:

$$\tau_{ij}^{\text{SGS}} = -C_s'^2 l^2 \left[2(2S_{mn}S_{mn})^{1/2}S_{ij} + C_1(S_{ik}S_{kj} - S_{mn}S_{mn}\delta_{ij}/3) + C_2(S_{ij}R_{kj} - R_{ik}S_{kj}) \right] \tag{5}$$

where S_{ij}, R_{ij}, δ_{ij} represents the resolved strain rate tensor, resolved rotation rate tenor, and Kronecker delta, respectively. The constants followed Mirocha et al. (2010). We further conducted the simulations based on these different turbulence schemes together with the cumulus convection schemes.

2.2. Experiment Design

The study evaluates the impact of cumulus and turbulence parameterization schemes on precipitation forecasts for three typhoon events, including Typhoon Mujigae (2015), Typhoon Hato (2017), and Typhoon Mangkhut (2018) using the WRF model, and the impact on intense precipitation predictions was relatively significant for the first two cases. We conducted simulations on three nested domains with grid resolutions of 15, 5, and 1.67 km, respectively; the model top is at 50 hPa with 50 vertical levels. Figure S1 in Supporting Information S1 displays the WRF domain configuration. The ECMWF Fifth-Generation Reanalysis (ERA5) was employed as the initial and boundary conditions for the WRF model. We conducted distinct simulations with or without employing the Grell-Freitas (Grell-3) cumulus scheme for cumulus convection associated with different horizontal turbulence schemes. For vertical turbulent mixing in the PBL, the ACM2 is applied in all the simulations (Pleim, 2007). Table 1 lists the eight simulations for each typhoon case, and Table S1 in Supporting Information S1 provides the detailed configuration of the simulations for each typhoon case. The Grell-Freitas scheme (Freitas et al., 2020; Grell & Freitas, 2014) is suitable both for the coarse and kilo-meter scale resolution as it is a scale-aware scheme based on the method described by Arakawa et al. (2011); the Grell-3 scheme is a conventional cumulus scheme based on the Grell–Devenyi ensemble scheme and can spread subsidence effects to neighboring grid columns and is also suitable for high-resolution typhoon simulations (Grell & Dévényi, 2002).

Specifically, for the GF-GF-R (G3-G3-R) simulations, the horizontal turbulence scheme which is referred to as the RNA scheme is in conjunction with the cumulus convective scheme; for the GF-GF-S (G3-G3-S) simulations, the Smagorinsky scheme was applied, while no horizontal turbulence scheme was used in the GF-GF-N (G3-G3-N) simulations. In the GF-N-N (G3-N-N) simulations, neither a cumulus nor a horizontal mixing turbulence scheme was activated in the two inner domains; in the GF-N-R (G3-N-R) simulations, the RNA scheme is turned on for the horizontal turbulence scheme and no cumulus scheme is used. In this study, we evaluated the impact of these two convective schemes on typhoon precipitation forecasts. The cumulus convection scheme applied in the innermost domains is consistent with the scheme used in the outermost domain. Given that the impacts are comparatively subtle in Typhoon Mangkhut, we focus on Typhoon Mujigae and Typhoon Hato to show the effects of convection and turbulence schemes in the following analysis.
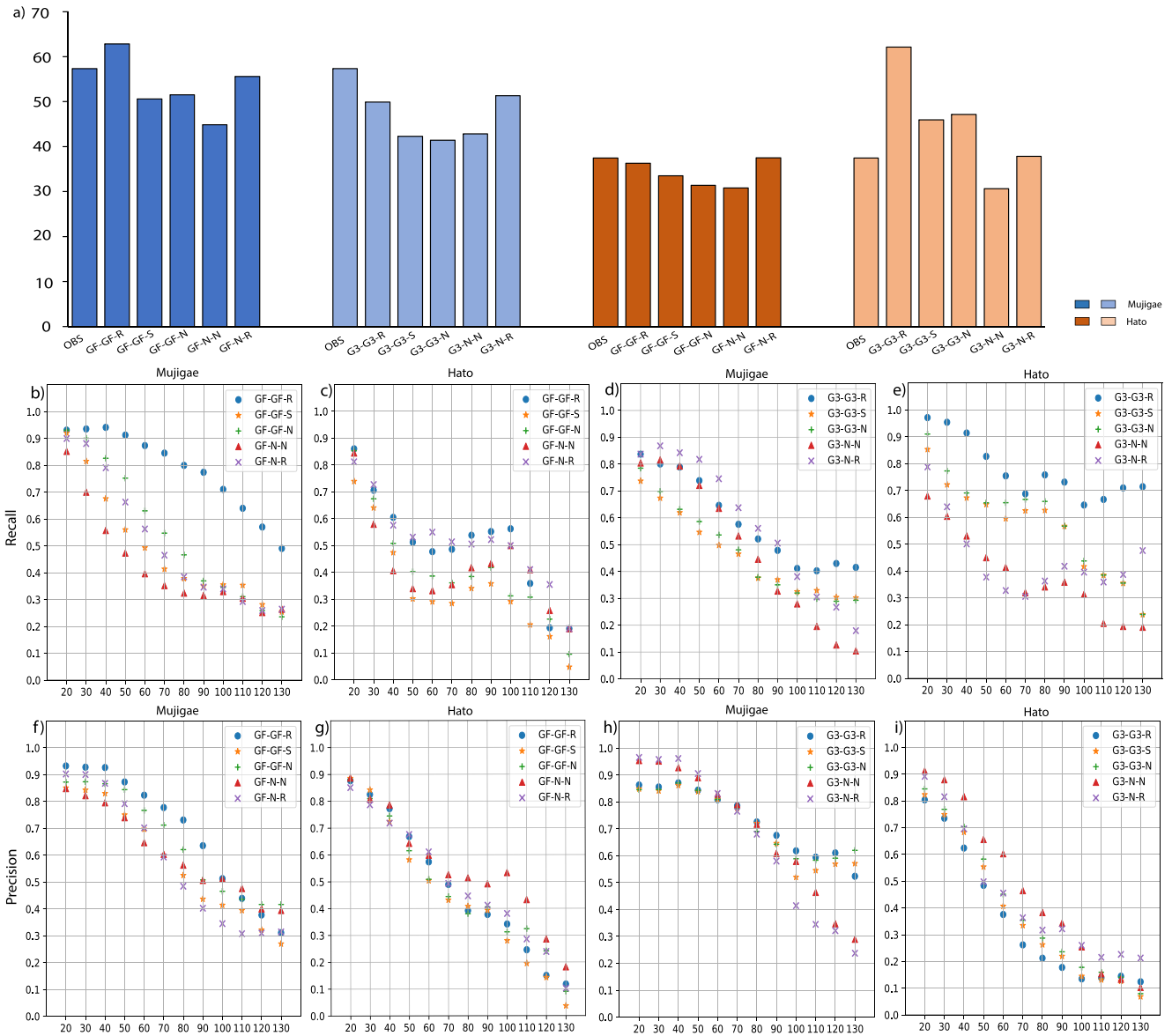
Figure 1. The averaged 24-hr accumulated precipitation in the innermost domain for Typhoon Mujigae and Typhoon Hato. The recall (b–e) and precision (f–i) scores for the 24-hr accumulated precipitation for simulations with different cumulus and turbulence schemes over observation at 1303 stations for Typhoon Mujigae (b, d, f, h) and Typhoon Hato (c, g, e, i) at different thresholds from 20 to 130 mm. (b, c, f, g): Grell–Freitas scheme, (d, h, e, i): Grell-3 scheme. Different turbulence schemes are shown using different symbols: blue dots represent the cumulus and RNA schemes; yellow stars represent the cumulus and Smagorinsky schemes; green crosses represent without applying a horizontal scheme, red triangles represent without applying cumulus and horizontal schemes and purple crosses represent applying the RNA scheme.

3. Results

3.1. Precipitation Forecast Evaluation

We compared the average precipitation from the 10 simulations in the innermost domain for each typhoon case with the observation from the 1303 ground-based stations in Guangdong province. The GF-N-R (G3-N-R) simulations produced more domain-averaged precipitation compared to the GF-N-N (G3-N-N) by applying RNA scheme separately (Figure 1a). The GF-N-R simulation for Typhoon Mujigae generated 58 mm accumulated precipitation which is close to the observation. In addition, the GF-GF-R and G3-G3-R simulations, which account for the cumulus and horizontal subgrid-scale turbulence, produced higher domain-averaged precipitation amounts compared to the other simulations without applying the cumulus schemes or RNA scheme. Specifically,

in the Mujigae case, the GF-GF-R simulation exhibited 48% more precipitation than the GF-N-N simulation and 24% more than the GF-GF-S (GF-GF-N) simulation. Moreover, applying the Smagorinsky scheme did not significantly impact the typhoon precipitation amount as demonstrated by similar domain-averaged precipitation in the GF-GF-N and G3-G3-N simulations. We also analyzed the distribution of 12-hr accumulated precipitation to examine the pattern of intense precipitation under different conditions, Figure S2 in Supporting Information S1 shows the results for Typhoon Mujigae. Although the overall typhoon structure in simulations using various schemes is similar, subtle differences exist in the rain band. The rain band is more compact, and the coverage of intense precipitation is more extensive in simulations that activate cumulus parameterization.

The recall and precision score for the 24-hr precipitation over 1303 stations in Guang Dong Province were calculated for the typhoon cases at different thresholds, from 20 to 130 mm. Recall denotes the ratio of correctly predicted extreme events to the actual occurrence of extreme precipitation, which measures the fraction of true-positive stations experiencing extreme events; precision represents the ratio of correctly predicted extreme events to simulated occurrences of extreme precipitation. The Typhoon Mujigae and Hato cases' precision and recall scores in simulations with different cumulus and horizontal turbulence schemes are shown in Figures 1b–1i. Focusing on the RNA scheme effect on the recall scores for the two cases, we found simulations applying the RNA scheme produced higher recall scores compared to simulations without applying any cumulus or horizontal turbulence scheme, showing a higher ability to catch the precipitation events in most cases, especially for the extreme precipitation events. The application of the Grell-3 or Grell-Freitas cumulus scheme simultaneously associated with the RNA scheme generated higher recall scores in most cases, especially in the threshold range of 40–100 mm, demonstrating the advantage in improving the hit rate of strong convection. For the Typhoon Mujigae case, the GF-GF-R simulation (Figure 1a) produced the highest recall score at all the thresholds compared with other simulations, displaying a three-times increase in recall compared to the GF-N-N simulation at the threshold of 80 mm. For the Typhoon Hato case, the difference in the recall score between the GF-GF-R and the GF-GF-N was less than 0.1 when the precipitation was less than 40 mm, and increased to 0.4 when accumulated precipitation exceeded 90 mm. In Figure 1d, in which the cumulus scheme is Grell-3, applying the RNA scheme showed significant advantages over simulations without applying the RNA scheme across all the thresholds. For Typhoon Mangkhut, applying the cumulus and RNA turbulence schemes showed limited effects on the precipitation simulation (Figure S6 in Supporting Information S1).

The impacts of the configuration of the RNA scheme with different cumulus schemes are inconsistent. In the Typhoon Mujigae case, the GF-GF-R performs better than the G3-G3-R in the Mujigae case, the Grell-Freitas scheme shows a 60% increase in recall compared to the Grell-3 scheme for the Mujigae case as shown in Figures 1b and 1d. The opposite result is found in the Typhoon Hato case. The simulation applying the Grell-3 scheme with the RNA scheme shows higher recall scores; the simulated precipitation in simulations using the Grell-Freitas scheme is comparable to those without applying the cumulus scheme. The results can be attributed to the Grell-Freitas scheme's reduced sensitivity to model resolution, leading to proportionately less precipitation at finer resolutions. The Grell-3 scheme is more sensitive to model resolution and produces more precipitation which aligns with findings from previous studies (Li et al., 2011). Concerning the precision score for Typhoon Mujigae (Figure 1f), the RNA scheme outperformed other schemes in predicting intense precipitation, accurately forecasting heavy rainfall lower than 90 mm. However, the RNA scheme lowered the precision scores above 100 mm. In conclusion, utilizing the cumulus and RNA schemes resulted in more accurate predictions of heavy rainfall, thereby improving the overall recall scores. However, it may also overestimate precipitation at some locations, leading to lower precision scores.

The relative error between the simulated accumulated precipitation and observed precipitation was calculated at thresholds of 60 and 120 mm to estimate the precipitation forecast performance for the different turbulence scheme configurations (Figure 2). Overall, the simulations using the RNA scheme for the horizontal turbulence show higher accuracy than others by decreasing the median relative error values at all the thresholds with both cumulus schemes. Simulations integrating the cumulus and RNA schemes outperform other simulations, especially for heavier hourly precipitation, which is consistent with the recall score in Figure 1. Specifically, the median value of the relative error of GF-GF-R (G3-G3-R) simulation is reduced by 52% (25%) than the GF-N-N (G3-N-N) simulation in Typhoon Mujigae at the 120 mm threshold (Figures 2b and 2d). Additionally, the relative error also shows opposite results with different cumulus schemes. The GF-GF-R simulation shows lower relative errors than the G3-G3-R in the Mujigea case (Figures 2a and 2b), which is 25% lower than the G3-G3-R
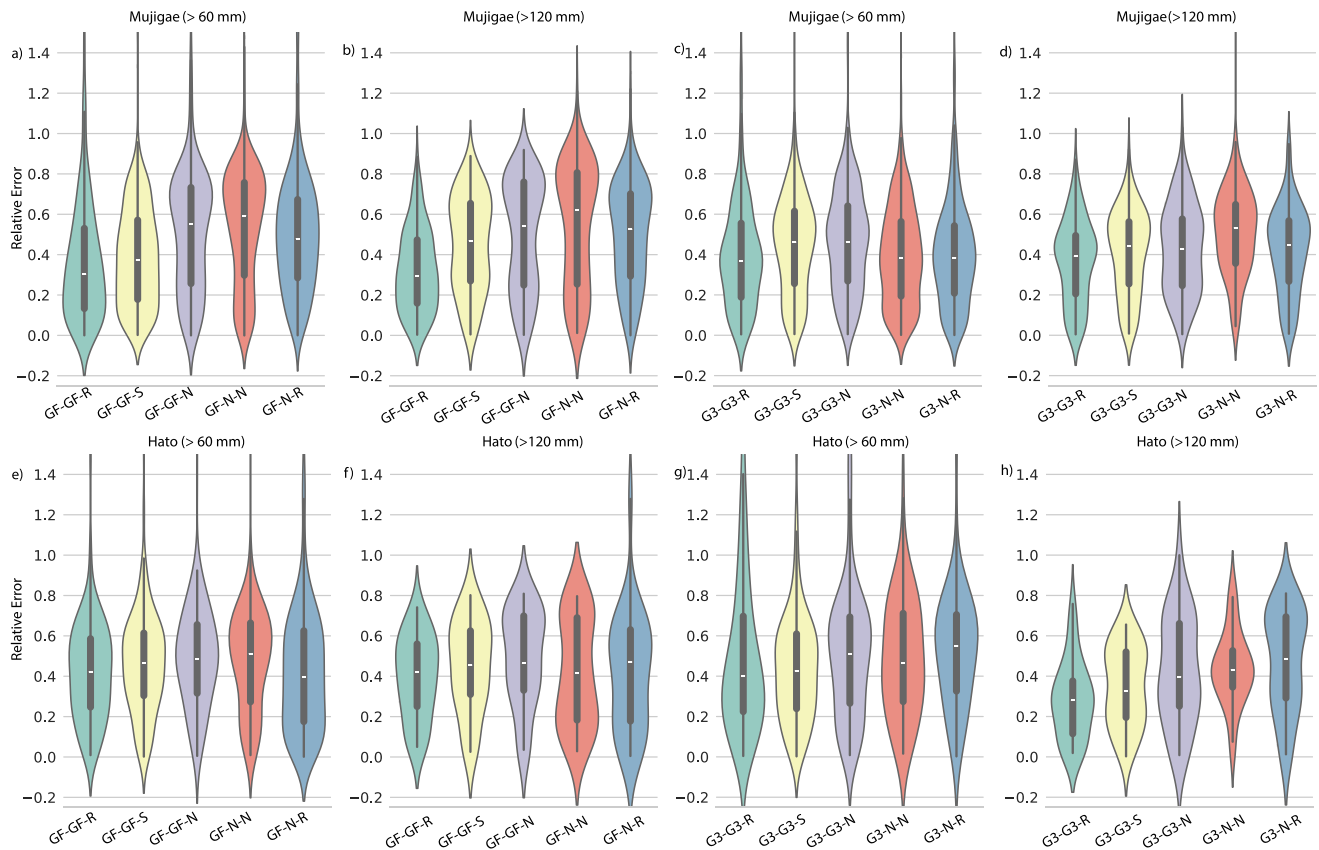
Figure 2. The relative error for the 24-hr accumulated precipitation for the different simulations over observation at 1303 stations for Typhoon Mujigae (a–d) and Typhoon Hato (e–h) at different thresholds (a, c, e, g) 60 mm, (b, d, f, h) 120 mm.

simulation at 120 mm threshold. However, the results are opposite to the Hato case (Figures 2f and 2h). Furthermore, applying the Smagorinsky scheme for horizontal turbulence tends to weaken the precipitation precision, producing larger errors than the GF-GF-N (G3-G3-N) simulation. It is noteworthy that the distribution of relative errors in the simulation results exhibits different characteristics, with a higher proportion of smaller relative errors observed in the simulation results employing the RNA scheme, suggesting that the utilization of the RNA scheme in the simulations not only produces a smaller median value but also reduces errors at more stations.

The simulated reflectivity of the different experiments and the observed reflectivity for Typhoon Hato at 03:00 UTC, 23 August, is shown in Figure 3 as an example to determine the impact on the typhoon's structure and strength. The G3-N-N simulation generates intense rainfall over the Hainan island in Figure 3e which is spurious compared with the observation, and simulations in Figures 3b–3d show relatively weak reflectivity at around 20 dBZ in Hainan island due to the more compact structure by adopting the cumulus and RNA schemes. In addition, the grid-point convection on the east in the G3-N-N simulation tends to be relatively small in the G3-G3-R simulation due to the stronger convection to deplete convective instability, indicating that simultaneously employing the RNA scheme and cumulus parameterization can maintain the structure and intensity of the typhoon and further avoid causing spurious precipitation. The same features are found in the reflectivity simulation of typhoon Mangkhut (Figure S3 in Supporting Information S1), where applying the Grell-3 parameterization eliminates the false rainfall falling in the north of the Guangdong Province and the Guangxi Province.

The minimum sea level pressure and maximum wind are analyzed to evaluate the impact of the RNA scheme on the typhoon intensity and location (Figure S4 in Supporting Information S1). Applying the RNA scheme enhanced the typhoon intensity for Typhoon Hato and Typhoon Mujigae, showing lower sea level pressure during the prelanding period. For instance, the sea level pressure of typhoon Hato reaches 950 hPa in the G3-G3-R and G3-N-R simulations, which is more intense than other simulations. The G3-G3-N and G3-G3-S simulations
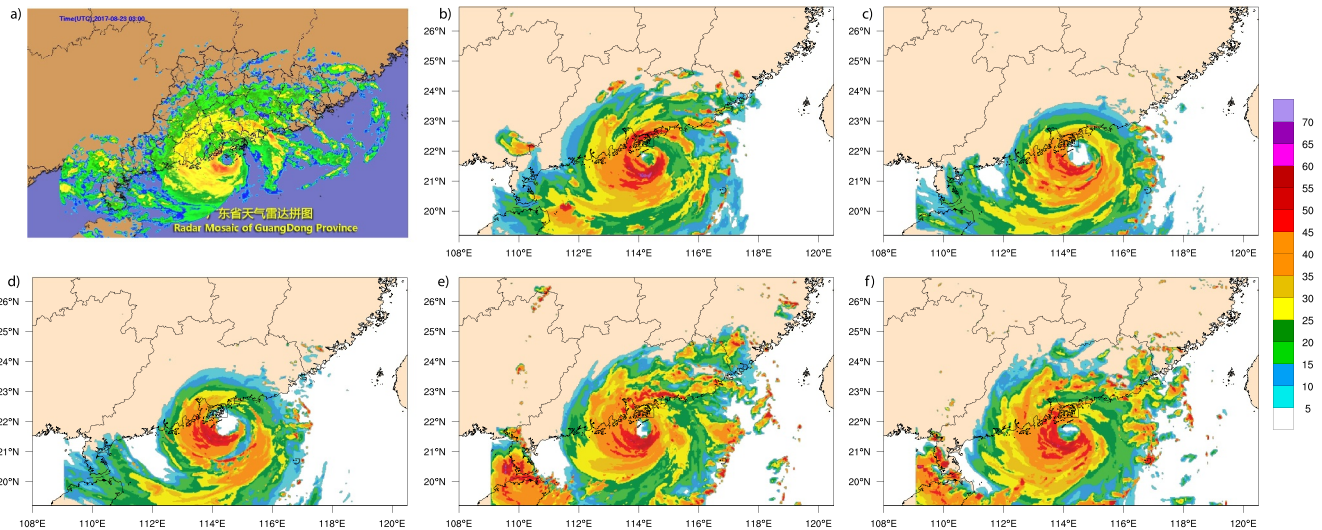
Figure 3. The observed and simulated reflectivity in different simulations for Typhoon Hato: (a) Observation, (b) G3-G3-R, (c) G3-G3-S, (d) G3-G3-N, (e) G3-N-N, (f) G3-N-R.

applying the Grell-3 cumulus scheme didn't show a significant difference in the sea level pressure compared with the G3-N-N (GF-N-N) simulation. On the other hand, the impact of the RNA and cumulus schemes on typhoon tracks is limited. Applying the cumulus and RNA schemes resulted in a higher maximum wind speed than other simulations. However, the G3-N-R simulation, which applies the RNA scheme alone, produces maximum wind speeds comparable to those of the G3-N-N (GF-N-N) simulation. It should be noted that the observations are based on best-track data and the comparison is not conducted at identical locations for both the observation and the simulation, satellite observations may provide further insights for evaluating wind speed over sea areas.

We further investigated the typhoon structure from the tangential and radial flow fields for the Typhoon Hato case (Figure S5 in Supporting Information S1). Applying the cumulus scheme yields a larger high wind speed radius in the G3-G3-R, G3-G3-N, and G3-G3-S simulations. The maximum tangential wind is also larger in the G3-G3-R case, which reaches 56 m/s, notably larger than the other simulations. Combining the RNA scheme and cumulus schemes produces stronger radial wind inflow, but simulations only applying RNA (G3-N-R) remain unchanged radial wind, which is consistent with the maximum wind. Furthermore, the depth of the radial inflow in the G3-G3-R simulation reaches 875 hPa, which is much larger than other simulations (975 hPa). In conclusion, applying the cumulus and RNA schemes simultaneously leads to larger intensity with a larger radius of maximum wind and deeper radial inflow.

3.2. Dynamical Analysis

The difference in convection intensity is mainly due to the interactions between the parameterized turbulence and the resolved flows. The product of parameterized flux and gradients can be used to measure the downgradient or upgradient generated by the horizontal turbulence parameterization (Shi et al., 2018). The parameterized horizontal mixing of potential temperature (θ) is measured by

$$\mathbf{\Pi_\theta} = -\tau_{\theta j}\frac{\partial \theta}{\partial x_j} \qquad (6)$$

where $\tau_{\theta j}$ is the parameterized horizontal turbulence flux of θ. This term can also produce or destroy the turbulence potential energy in the governing equation of the sub-filter scale θ variance (Shi, Enriquez, et al., 2019).

For the downgradient or upgradient mixing of the momentum can be measured by
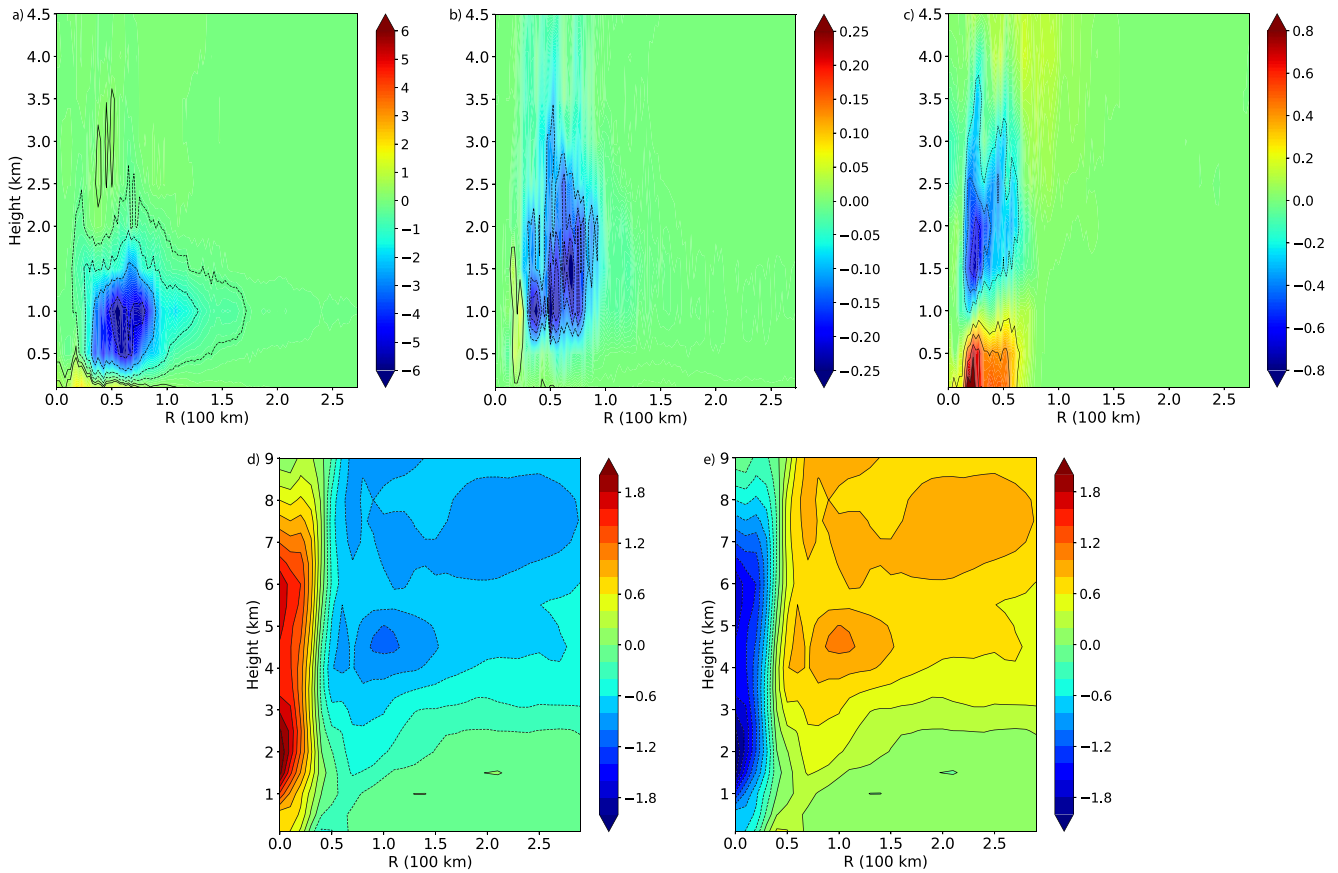
Figure 4. Time-averaged dynamics and difference in simulated potential temperature under different cumulus schemes for the 6 hr before landing. Panels (a–c) display the energy dissipation (positive) and backscatter (negative) within the G3-G3-R simulations for Typhoon Hato: (a) horizontal momentum, (b) vertical velocity, and (c) variance of potential temperature. Panels (d and e) show the difference in potential temperature for different cumulus schemes: (d) Grell-Freitas and (e) Grell-3.

$$\Pi = -\tau_{ij}\frac{\partial u_i}{\partial x_j} = -\tau_{ij}S_{ij} \tag{7}$$

We can divide it into the horizontal and vertical momentum components. For the Π_h, $i = 1,2$ and $j = 1,2$, for the vertical component, $i = 3$ and $j = 1,2$. The positive and negative values represent the downgradient and upgradient mixing of the momentum, respectively. We show the momentum and potential temperature mixing in typhoon Hato in Figures 4a–4c. The mixing of the horizontal momentum shows larger negative values, meaning the RNA scheme generated upgradient mixing around 2 km. In contrast, the value above 2 km is positive with a much smaller magnitude, which implies weak downgradient (dissipation) transport happened. From the tangential wind analysis, we found that only applying the RNA scheme leads to a larger height of the maximum tangential wind than the G3-N-R simulation. By combining the cumulus and the RNA schemes, the maximum tangential wind height reaches 925 hPa. This demonstrates that the RNA scheme enhanced the low-level wind through backscattering. Moreover, the upgradient transport of the horizontal turbulence which enhanced the tangential wind can further enhance the convection in the secondary circulation by the dynamical adjustment. In Figure 4b, we also found the significant backscattering extended to 3 km, suggesting the upgradient transportation of the vertical velocity, which also favors the convection development in the typhoon eyewall. The flux shows the same configuration in other typhoon cases, although the effect is relatively weaker.

Figure 4c shows the calculated heat variance dissipation for the RNA scheme as a function of height and the radius from the typhoon center for Typhoon Hato. We can see that Π_θ displayed positive values meaning downgradient mixing at the low height level. The height of the downgradient mixing of potential temperature extends to 1 km in

typhoon cases. On the other hand, the heat flux is upgradient at high levels, indicated by the positive Π_θ values. As a result, the high-entropy air is transported from the eyewall to the outside, which further enhances the buoyancy of the updraft in the eyewall; in contrast, the backscattering at the upper level seems to be advantageous for deepening the convection, as it may potentially reduce the entrainment of environmental air, which will be investigated with further numerical experiments. In addition, different typhoon intensities may induce different magnitudes of heat and momentum fluxes, for example, the heat flux of Typhoon Hato is stronger than Typhoon Mujigae. Nevertheless, both fluxes configurations contribute to the increased precipitation intensity, consistent with the enhanced typhoon precipitation forecast in the G3-G3-R simulations. The tangential wind is stronger near the eyewall in the G3-G3-R simulations than in the others. However, the G3-N-N simulation can produce stronger tangential wind in some situations, as in the Typhoon Hato Case.

We also examined the impact of different cumulus schemes by analyzing the difference in the potential temperature between the GF-GF-N and G3-G3-N simulations and their averaged field. We show the difference as a function of the radius from the center 6 hr before landing in Figures 4d and 4e. The Grell-3 scheme shows warmer air at the high level because the high entropy air from lower levels and the eye is transported to the environment and leads to more intense precipitation, resulting in higher recall scores and lower relative error in the heavy rainfall scale compared to the Grell-Freitas simulation. In addition, we found the moisture convergence in the G3-G3-N simulation is stronger than the GF-GF-N simulation for Typhoon Hato, especially before the landing stage, which means the Grell-3 scheme leads to intensified convection which is close to the observation. But for Typhoon Mujigae, allying the Grell-Freitas results in weaker moisture convergence which is consistent with the precipitation forecasts. However, as we mentioned before, the performance of the schemes can vary in different cases because of the various environments and typhoon structures, and the adaptation of the cumulus for the gray zone scheme still needs further investigation.

4. Conclusion

Tropical cyclones are significant weather systems, leading to extreme rainfall in coastal areas. Although convection-permitting-resolution numerical predictions of typhoons have become operational in many regions, forecasting precipitation remains challenging due to the controversial representation of convection and turbulence at gray zone resolutions. Traditional boundary layer turbulence schemes do not allow for horizontal turbulence, which might hinder accurate typhoon precipitation predictions. Nevertheless, recent research has emphasized the importance of both vertical and horizontal subgrid-scale effects in the simulation of typhoon development. This study evaluated the necessity and efficacy of the cumulus and RNA turbulence schemes on typhoon precipitation in kilometer-scale resolution simulations in border typhoon cases.

We found that applying the RNA turbulence scheme and integrating the cumulus scheme and turbulence scheme led to increased domain-averaged precipitation, higher recall scores, and reduced relative error compared to other simulations. Applying the cumulus and RNA turbulence schemes can enhance the typhoon intensity and generate more compact structures with lower minimum sea level pressure, and higher maximum wind speed. Combining the cumulus and RNA schemes also leads to a larger radius of maximum wind and deeper radial inflow which benefit the intense convection. In addition, the two cumulus schemes exhibit varying impacts when integrated with the RNA scheme due to the specific characteristics of the schemes and typhoon cases. However, implementing the convection parameterization and RNA turbulence schemes does not necessarily enhance precipitation forecasting for weak precipitation events. The RNA scheme can generate horizontal downgradient mixing of potential temperature, increasing buoyancy flow toward the eyewall. Simultaneously, backscatter is observed in the upper level, reducing the convection core's depletion. The RNA scheme also promotes the upgradient transport of momentum in the lower troposphere, dynamically reinforcing typhoon circulation. We noticed that the magnitude of momentum and flux varies due to differing typhoon intensities, but the overall trend remains consistent.

Our study highlights the importance of considering cumulus and horizontal subgrid-scale turbulence impacts in typhoon precipitation forecasts at convection-permitting resolutions, particularly for extreme precipitation events. They are useful to improve heavy rainfall warnings for typhoon cases. However, the specific impact of the RNA scheme and the advantage of the scale-aware convection scheme varies in different typhoon cases, probably related to the distinct boundary layer environments, background fields, the sensitivity of combining the micro-physical and cumulus scheme, the specific entrainment and typhoon structures of different cases. The results are

also consistent with previous studies, Liu et al. (2020) found that only the Grell-3 is superior for accumulated rainfall simulation in the central Tianshan Mountains; Jeworrek et al. (2019) showed that GF performed better in the two case studies in the US Southern Great Plains. Ensemble numerical simulations will be conducted to investigate the cumulus and RNA turbulence parameterization schemes across different grid-resolution scales for typhoons exhibiting varying structures and intensities.

Data Availability Statement

The Weather Research and Forecast model is publicly available at https://github.com/shixm-cloud/WRF-RNA. We archived the namelist for our simulations in Wang (2024).

References

Arakawa, A., Jung, J.-H., & Wu, C.-M. (2011). Toward unification of the multiscale modeling of the atmosphere. *Atmospheric Chemistry and Physics*, *11*(8), 3731–3742. https://doi.org/10.5194/acp-11-3731-2011

Boutle, I., Eyre, J., & Lock, A. (2014). Seamless stratocumulus simulation across the turbulent gray zone. *Monthly Weather Review*, *142*(4), 1655–1668. https://doi.org/10.1175/mwr-d-13-00229.1

Carper, M. A., & Porté-Agel, F. (2004). The role of coherent structures in subfilter-scale dissipation of turbulence measured in the atmospheric surface layer. *Journal of Turbulence*, *5*(1), 040. https://doi.org/10.1088/1468-5248/5/1/040

Chow, F. K., Street, R. L., Xue, M., & Ferziger, J. H. (2005). Explicit filtering and reconstruction turbulence modeling for large-eddy simulation of neutral boundary layer flow. *Journal of the Atmospheric Sciences*, *62*(7), 2058–2077. https://doi.org/10.1175/jas3456.1

Freitas, S. R., Grell, G. A., & Li, H. (2020). The GF convection parameterization: Recent developments, extensions, and applications. *Geoscientific Model Development Discussions*, *2020*, 1–28.

Gao, Y., Leung, L. R., Zhao, C., & Hagos, S. (2017). Sensitivity of US summer precipitation to model resolution and convective parameterizations across gray zone resolutions. *Journal of Geophysical Research: Atmospheres*, *122*(5), 2714–2733. https://doi.org/10.1002/2016jd025896

Gerard, L. (2007). An integrated package for subgrid convection, clouds and precipitation compatible with meso-gamma scales. *Quarterly Journal of the Royal Meteorological Society: A Journal of the Atmospheric Sciences, Applied Meteorology and Physical Oceanography*, *133*(624), 711–730. https://doi.org/10.1002/qj.58

Grell, G. A., & Dévényi, D. (2002). A generalized approach to parameterizing convection combining ensemble and data assimilation techniques. *Geophysical Research Letters*, *29*(14), 38–41. https://doi.org/10.1029/2002gl015311

Grell, G. A., & Freitas, S. R. (2014). A scale and aerosol aware stochastic convective parameterization for weather and air quality modeling. *Atmospheric Chemistry and Physics*, *14*(10), 5233–5250. https://doi.org/10.5194/acp-14-5233-2014

Houze Jr, R. A. (2014). *Cloud dynamics*. Academic Press.

Jeworrek, J., West, G., & Stull, R. (2019). Evaluation of cumulus and microphysics parameterizations in WRF across the convective gray zone. *Weather and Forecasting*, *34*(4), 1097–1115. https://doi.org/10.1175/waf-d-18-0178.1

Kirkil, G., Mirocha, J., Bou-Zeid, E., Chow, F. K., & Kosović, B. (2012). Implementation and evaluation of dynamic subfilter-scale stress models for large-eddy simulation using WRF. *Monthly Weather Review*, *140*(1), 266–284. https://doi.org/10.1175/mwr-d-11-00037.1

Kosović, B. (1997). Subgrid-scale modelling for the large-eddy simulation of high-Reynolds-number boundary layers. *Journal of Fluid Mechanics*, *336*, 151–182. https://doi.org/10.1017/s0022112096004697

Li, W., Li, L., Fu, R., Deng, Y., & Wang, H. (2011). Changes to the North Atlantic subtropical high and its role in the intensification of summer rainfall variability in the southeastern United States. *Journal of Climate*, *24*(5), 1499–1506. https://doi.org/10.1175/2010jcli3829.1

Liu, Y., Chen, X., Li, Q., Yang, J., Li, L., & Wang, T. (2020). Impact of different microphysics and cumulus parameterizations in WRF for heavy rainfall simulations in the central segment of the Tianshan Mountains, China. *Atmospheric Research*, *244*, 105052. https://doi.org/10.1016/j.atmosres.2020.105052

Mahoney, K. M. (2016). The representation of cumulus convection in high-resolution simulations of the 2013 Colorado Front Range flood. *Monthly Weather Review*, *144*(11), 4265–4278. https://doi.org/10.1175/mwr-d-16-0211.1

Mirocha, J., Lundquist, J., & Kosović, B. (2010). Implementation of a nonlinear subfilter turbulence stress model for large-eddy simulation in the advanced research WRF model. *Monthly Weather Review*, *138*(11), 4212–4228. https://doi.org/10.1175/2010mwr3286.1

Pleim, J. E. (2007). A combined local and nonlocal closure model for the atmospheric boundary layer. Part I: Model description and testing. *Journal of Applied Meteorology and Climatology*, *46*(9), 1383–1395. https://doi.org/10.1175/jam2539.1

Shi, X., Chow, F. K., Street, R. L., & Bryan, G. H. (2019). Key elements of turbulence closures for simulating deep convection at kilometer-scale resolution. *Journal of Advances in Modeling Earth Systems*, *11*(3), 818–838. https://doi.org/10.1029/2018ms001446

Shi, X., Enriquez, R. M., Street, R. L., Bryan, G. H., & Chow, F. K. (2019). An implicit algebraic turbulence closure scheme for atmospheric boundary layer simulation. *Journal of the Atmospheric Sciences*, *76*(11), 3367–3386. https://doi.org/10.1175/jas-d-18-0375.1

Shi, X., Hagen, H. L., Chow, F. K., Bryan, G. H., & Street, R. L. (2018). Large-eddy simulation of the stratocumulus-capped boundary layer with explicit filtering and reconstruction turbulence modeling. *Journal of the Atmospheric Sciences*, *75*(2), 611–637. https://doi.org/10.1175/jas-d-17-0162.1

Shi, X., & Wang, Y. (2022). Impacts of cumulus convection and turbulence parameterizations on the convection-permitting simulation of typhoon precipitation. *Monthly Weather Review*, *150*(11), 2977–2997. https://doi.org/10.1175/mwr-d-22-0057.1

Skamarock, W. C., Klemp, J. B., Dudhia, J., Gill, D. O., Barker, D. M., Duda, M. G., et al. (2008). A description of the advanced research WRF version 3. *NCAR technical note*, *475*, 113.

Stolz, S., & Adams, N. A. (1999). An approximate deconvolution procedure for large-eddy simulation. *Physics of Fluids*, *11*(7), 1699–1701. https://doi.org/10.1063/1.869867

Stolz, S., Adams, N. A., & Kleiser, L. (2001). An approximate deconvolution model for large-eddy simulation with application to incompressible wall-bounded flows. *Physics of Fluids*, *13*(4), 997–1015. https://doi.org/10.1063/1.1350896

Sun, Y., Yi, L., Zhong, Z., & Ha, Y. (2014). Performance of a new convective parameterization scheme on model convergence in simulations of a tropical cyclone at grey-zone resolutions. *Journal of the Atmospheric Sciences*, *71*(6), 2078–2088. https://doi.org/10.1175/jas-d-13-0285.1

Sun, Y., Yi, L., Zhong, Z., Hu, Y., & Ha, Y. (2013). Dependence of model convergence on horizontal resolution and convective parameterization in simulations of a tropical cyclone at gray-zone resolutions. *Journal of Geophysical Research: Atmospheres*, *118*(14), 7715–7732. https://doi.org/10.1002/jgrd.50606

Wang, Y. (2024). Namelists for the experiments [Dataset]. *Zenodo*. https://doi.org/10.5281/zenodo.10989959

Weisman, M. L., Skamarock, W. C., & Klemp, J. B. (1997). The resolution dependence of explicitly modeled convective systems. *Monthly Weather Review*, *125*(4), 527–548. https://doi.org/10.1175/1520-0493(1997)125<0527:trdoem>2.0.co;2

Wyngaard, J. C. (2004). Toward numerical modeling in the "terra incognita". *Journal of the Atmospheric Sciences*, *61*(14), 1816–1826. https://doi.org/10.1175/1520-0469(2004)061<1816:tnmitt>2.0.co;2

Yu, X., & Lee, T.-Y. (2011). Role of convective parameterization in simulations of heavy precipitation systems at grey-zone resolutions—Case studies. *Asia-Pacific Journal of Atmospheric Sciences*, *47*(2), 99–112. https://doi.org/10.1007/s13143-011-0001-3

Zhou, B., Zhu, K., & Xue, M. (2017). A physically based horizontal subgrid-scale turbulent mixing parameterization for the convective boundary layer. *Journal of the Atmospheric Sciences*, *74*(8), 2657–2674. https://doi.org/10.1175/jas-d-16-0324.1